Vertically-oriented nanoparticle dimer based on focused plasmonic trapping

Zhe Shen,[1] Lei Su,[2] and Yao-chun Shen[1,*]

[1]*Department of Electrical Engineering & Electronics, University of Liverpool, Liverpool L69 3GJ, United Kingdom*
[2]*School of Engineering and Materials Science, Queen Mary University of London, London E1 4NS, United Kingdom*

Abstract: We proposed a vertically-oriented dimer structure based on focused plasmonic trapping of metallic nanoparticle. Quantitative FDTD calculations and qualitative analysis by simplified dipole approximation revealed that localized surface plasmon coupling dominates in the plasmon hybridization, and the vertically-oriented dimer can effectively make use of the dominant longitudinal component of the surface plasmon virtual probe thus providing much stronger electric field in the gap. Furthermore, for practical application the top nanoparticle of the dimer can be replaced with an atomic force microscope tip which enables the precise control of the gap distance of the dimer. Therefore the proposed vertically-oriented dimer structure provides both the scanning capability and the extremely-high electrical field necessary for the high sensitivity Raman imaging.

References and links

1. C. E. Talley, J. B. Jackson, C. Oubre, N. K. Grady, C. W. Hollars, S. M. Lane, T. R. Huser, P. Nordlander, and N. J. Halas, "Surface-enhanced Raman scattering from individual Au nanoparticles and nanoparticle dimer substrates," Nano Lett. **5**, 1569-1574 (2005).
2. W. Li, P. H. Camargo, X. Lu, and Y. Xia, "Dimers of silver nanospheres: facile synthesis and their use as hot spots for surface-enhanced Raman scattering," Nano Lett. **9**, 485-490 (2009).
3. K. D. Alexander, K. Skinner, S. P. Zhang, H. Wei, and R. Lopez, "Tunable SERS in Gold Nanorod Dimers through Strain Control on an Elastomeric Substrate," Nano Lett. **10**, 4488-4493 (2010).
4. J. Jiao, X. Wang, F. Wackenhut, A. Horneber, L. Chen, A. V. Failla, A. J. Meixner, and D. Zhang, "Polarization-dependent SERS at differently oriented single gold nanorods," Chemphyschem : a European journal of chemical physics and physical chemistry **13**, 952-958 (2012).
5. A. Kinkhabwala, Z. F. Yu, S. H. Fan, Y. Avlasevich, K. Mullen, and W. E. Moerner, "Large single-molecule fluorescence enhancements produced by a bowtie nanoantenna," Nat. Photonics **3**, 654-657 (2009).
6. N. A. Hatab, C. H. Hsueh, A. L. Gaddis, S. T. Retterer, J. H. Li, G. Eres, Z. Zhang, and B. Gu, "Free-standing optical gold bowtie nanoantenna with variable gap size for enhanced Raman spectroscopy," Nano Lett. **10**, 4952-4955 (2010).
7. K. Fujita, S. Ishitobi, K. Hamada, N. I. Smith, A. Taguchi, Y. Inouye, and S. Kawata, "Time-resolved observation of surface-enhanced Raman scattering from gold nanoparticles during transport through a living cell," J. Biomed. Opt. **14**, 024038 (2009).
8. E. Bailo, and V. Deckert, "Tip-enhanced Raman spectroscopy of single RNA strands: towards a novel direct-sequencing method," Angewandte Chemie **47**, 1658-1661 (2008).
9. J. F. Shen, J. Wang, C. J. Zhang, C. J. Min, H. Fang, L. P. Du, S. W. Zhu, and X. C. Yuan, "Dynamic plasmonic tweezers enabled single-particle-film-system gap-mode Surface-enhanced Raman scattering," Appl. Phys. Lett. **103**, 191119 (2013).
10. L. P. Du, D. Y. Tang, G. H. Yuan, S. B. Wei, and X. C. Yuan, "Emission pattern of surface-enhanced Raman scattering from single nanoparticle-film junction," Appl. Phys. Lett. **102**, 081117 (2013).
11. K. Uetsuki, P. Verma, P. Nordlander, and S. Kawata, "Tunable plasmon resonances in a metallic nanotip-film system," Nanoscale **4**, 5931-5935 (2012).
12. E. G. Bortchagovsky, S. Klein, and U. C. Fischer, "Surface plasmon mediated tip enhanced Raman scattering," Appl. Phys. Lett. **94**, 063118 (2009).
13. K. Kneipp, Y. Wang, H. Kneipp, L. T. Perelman, I. Itzkan, R. Dasari, and M. S. Feld, "Single molecule detection using surface-enhanced Raman scattering (SERS)," Phys. Rev. Lett. **78**, 1667-1670 (1997).
14. E. Hao and G. C. Schatz, "Electromagnetic fields around silver nanoparticles and dimers," Journal of Chemical Physics **120**, 357-366 (2004).
15. G. Volpe, R. Quidant, G. Badenes, and D. Petrov, "Surface plasmon radiation forces," Phys. Rev. Lett. **96**, 238101 (2006).
16. M. Righini, A. S. Zelenina, C. Girard, and R. Quidant, "Parallel and selective trapping in a patterned plasmonic landscape," Nat. Phys. **3**, 477-480 (2007).

17. M. Righini, G. Volpe, C. Girard, D. Petrov, and R. Quidant, "Surface plasmon optical tweezers: tunable optical manipulation in the femtonewton range," Phys. Rev. Lett. **100**, 186804 (2008).
18. K. Wang, E. Schonbrun, and K. B. Crozier, "Propulsion of Gold Nanoparticles with Surface Plasmon Polaritons: Evidence of Enhanced Optical Force from Near-Field Coupling between Gold Particle and Gold Film," Nano Lett. **9**, 2623-2629 (2009).
19. W. Zhang, L. Huang, C. Santschi, and O. J. F. Martin, "Trapping and Sensing 10 nm Metal Nanoparticles Using Plasmonic Dipole Antennas," Nano Lett. **10**, 1006-1011 (2010).
20. M. L. Juan, M. Righini, and R. Quidant, "Plasmon nano-optical tweezers," Nat. Photonics **5**, 349-356 (2011).
21. Z. Shen and L. Su, "Plasmonic trapping and tuning of a gold nanoparticle dimer," Opt. Express **24**, 4801-4811 (2016) .
22. C. Oubre, and P. Nordlander, "Finite-difference time-domain studies of the optical properties of nanoshell dimers," Journal of Physical Chemistry B **109**, 10042-10051 (2005).
23. A. Polemi, and K. L. Shuford, "Distance dependent quenching effect in nanoparticle dimers," Journal of Chemical Physics **136** (2012).
24. C. Min, Z. Shen, J. Shen, Y. Zhang, H. Fang, G. Yuan, L. Du, S. Zhu, T. Lei, and X. Yuan, "Focused plasmonic trapping of metallic particles," Nat. Commun. **4**, 2891 (2013).
25. Q. W. Zhan, "Evanescent Bessel beam generation via surface plasmon resonance excitation by a radially polarized beam," Opt. Lett. **31**, 1726-1728 (2006).
26. W. B. Chen, and Q. W. Zhan, "Realization of an evanescent Bessel beam via surface plasmon interference excited by a radially polarized beam," Opt. Lett. **34**, 722-724 (2009).
27. L. Novotny and B. Hecht, *Principles of Nano-optics* (Cambridge University, 2012).
28. B. Richards and E. Wolf, "Electromagnetic diffraction in optical systems .2. Structure of the image field in an aplanatic system," Proc. R. Soc. A. **253**, 358-379 (1959).
29. G. Leveque, and O. J. F. Martin, "Optical interactions in a plasmonic particle coupled to a metallic film," Opt. Express **14**, 9971-9981 (2006).
30. A. Farhang, N. Bigler, and O. J. F. Martin, "Coupling of multiple LSP and SPP resonances: interactions between an elongated nanoparticle and a thin metallic film," Opt. Lett. **38**, 4758-4761 (2013).
31. P. Nordlander, and E. Prodan, "Plasmon Hybridization in Nanoparticles near Metallic Surfaces," Nano Lett. **4**, 2209-2213 (2004).
32. F. Le, N. Z. Lwin, N. J. Halas, and P. Nordlander, "Plasmonic interactions between a metallic nanoshell and a thin metallic film," Phys. Rev. B **76**, 165410 (2007).
33. N. Papanikolaou, "Optical properties of metallic nanoparticle arrays on a thin metallic film," Phys. Rev. B **75**, 235426 (2007).
34. Y. P. Wu, and P. Nordlander, "Finite-Difference Time-Domain Modeling of the Optical Properties of Nanoparticles near Dielectric Substrates," J. Phys. Chem. C **114**, 7302-7307 (2010).
35. H. Wang, T. Liu, Y. Z. Huang, Y. R. Fang, R. C. Liu, S. X. Wang, W. J. Wen, and M. T. Sun, "Plasmon-driven surface catalysis in hybridized plasmonic gap modes," Sci. Rep. **4**, 7087 (2014).
36. Y. Q. Zhang, W. Shi, Z. Shen, Z. S. Man, C. J. Min, J. F. Shen, S. W. Zhu, H. P. Urbach, and X. C. Yuan, "A Plasmonic Spanner for Metal Particle Manipulation," Sci. Rep. **5**, 15446 (2015).
37. Y. Q. Zhang, J. Wang, J. F. Shen, Z. S. Man, W. Shi, C. J. Min, G. H. Yuan, S. W. Zhu, H. P. Urbach, and X. C. Yuan, "Plasmonic Hybridization Induced Trapping and Manipulation of a Single Au Nanowire on a Metallic Surface," Nano Lett. **14**, 6430-6436 (2014).
38. A. A. E. Saleh, and J. A. Dionne, "Toward Efficient Optical Trapping of Sub-10-nm Particles with Coaxial Plasmonic Apertures," Nano Lett. **12**, 5581-5586 (2012).
39. A. H. J. Yang, T. Lerdsuchatawanich, and D. Erickson, "Forces and Transport Velocities for a Particle in a Slot Waveguide," Nano Lett. **9**, 1182-1188 (2009).
40. S. Albaladejo, R. Gómez-Medina, L. S. Froufe-Pérez, H. Marinchio, R. Carminati, J. F. Torrado, G. Armelles, A. García-Martín, and J. J. Sáenz, "Radiative corrections to the polarizability tensor of an electrically small anisotropic dielectric particle," Opt. Express **18**, 3556-3567 (2010).
41. C. F. Bohren and D. R. Huffman, *Absorption and Scattering of Light by Small Particles* (Wiley, 1983).
42. A. Pinchuk and G. Schatz, "Anisotropic polarizability tensor of a dimer of nanospheres in the vicinity of a plane substrate," Nanotechnology **16**, 2209-2217 (2005).
43. V. V. Gozhenko, L. G. Grechko, and K. W. Whites, "Electrodynamics of spatial clusters of spheres: Substrate effects," Phys. Rev. B **68**, 125422 (2003).
44. Y. S. Touloukian, *Thermal Conductivity: Metallic Elements and Alloys* (IFI/Plenum, 1970).
45. K. C. Neuman, and S. M. Block, "Optical trapping," Rev. Sci. Instrum. **75**, 2787-2809 (2004).
46. A. H. J. Yang, T. Lerdsuchatawanich, and D. Erickson, "Forces and Transport Velocities for a Particle in a Slot Waveguide," Nano Lett. **9**, 1182-1188 (2009).
47. E. L. Florin, A. Pralle, E. H. K. Stelzer, and J. K. H. Horber, "Photonic force microscope calibration by thermal noise analysis," Appl. Phys. A. **66**, S75-S78 (1998).
48. L. I. McCann, M. Dykman, and B. Golding, "Thermally activated transitions in a bistable three-dimensional optical trap," Nature **402**, 785-787 (1999).
49. E. C. Le Ru and P. G. Etchegoin, "Rigorous justification of the [E](4) enhancement factor in Surface Enhanced Raman Spectroscopy," Chem. Phys. Lett. **423**, 63-66 (2006).

1. Introduction

Metallic nanostructures have been intensively studied both theoretically and experimentally. Due to the interaction between the incident photons and the free electrons in the metallic nanostructures, plasmon resonance can be generated at the vicinity of the nanostructure and an enhanced electrical field can be observed. A typical application is on surface enhanced Raman scattering (SERS) where the metallic nanostructures lead to significantly increase Raman signals. These metallic nanostructures can be simply divided into horizontal and vertical orientations. Horizontal direction structures can be in the form of horizontal-oriented nanoparticle dimer [1,2], nanorods antenna [3,4] and bow-tie nanostructure [5,6]. Vertical direction structures include nanoparticle-dielectric substrate [7], tip-dielectric substrate [8], nanoparticle-film [9,10] and tip-film [11,12]. Compared to horizontally-oriented structures, vertically-oriented structures provide additional benefit of scanning capability. Therefore, vertically-oriented structures have great potential in the area of scanning Raman imaging.

The ability to detect single molecules in solution with high sensitivity and molecular specificity is of great scientific and practical interest in many fields such as chemistry, biology, medicine, pharmacology and environmental science. Single molecule detection using SERS was first achieved using nanoparticles where the Raman signal enhancement can be explained as simple localized surface plasmon (LSP) [13]. It has been shown that gap mode nanostructures such as horizontally- or vertically-oriented dimers provide much greater Raman enhancement, owing to the surface plasmon polarition (SPP) and LSP coupling (SPP-LSP coupling) or LSP-LSP coupling. The hot spot in the gap of the dimer is outstanding, as the electrical field enhancement created from the LSPs hybridization could be three orders of magnitude larger than that from monomers, depends on the shape, size, and orientation of the nanoparticles [14]. Horizontally-oriented dimer structures can be physically fabricated and/or assembled on a plane substrate using nanofabrication techniques and they have been a subject of extensive investigations [3-6]. For dynamic control of the forming of the dimer structure, plasmonic trapping of nanoparticle is a promising technique [15-20]. Very recently we have shown that horizontally-oriented dimer structures can also be generated through plasmonic trapping with virtual probe pairs [21]. However, these horizontally-oriented dimer structures have no scanning capability thus they are not suitable for high-resolution Raman spectroscopy imaging applications. Here we propose to use a novel vertically-oriented dimer nanostructure for high-sensitivity and high-resolution SERS imaging.

In addition, the axis orientation of the dimer structure is of significant importance since the coupling efficiency reaches its maximum when the polarization of the incident light is aligned parallel to the axis of the dimer structures [22,23]. Usually the focal light field has transverse and longitudinal components. The horizontally-oriented and vertically-oriented dimers are sensitive to transverse and longitudinal components, respectively. Particularly for high-order laser mode such as radially polarized beam, its longitudinal component is dominant after focusing. The vertically-oriented dimer will be able to take this advantages thus provides even stronger Raman signal enhancement.

In this paper, we proposed a vertically-oriented dimer, e.g., a particle-particle-film system which serves as a simple conceptual model for revealing the electrical field enhancement underlying SERS application. In this vertically-oriented dimer system the bottom nanoparticle is immobilized above the Ag film by the plasmonic trapping method introduced in our previous work [24] and the top nanoparticle can be regarded as the atom force microscopy (AFM) tip which enables precise locating above the bottom particle. The gap distance of the dimer can thus be accurately adjusted by the AFM tip. We will show that surface plasmon virtual probe (SP-VP) could be a great candidate in building vertical nanostructure system. On the one hand, SP-VP can provide strong gradient force which allows the bottom nanoparticle to be manipulated. On the other hand, SP-VP has dominant longitudinal component [25,26] which couples very efficiently with the vertically-oriented dimers thus provide further

improvement of the Raman enhancement. In this work, we first derived the field distribution of SP-VP excited by focused radially polarized beam (RPB). Maxwell stress tensor (MST) method is then applied to calculate the force based on the finite difference time domain (FDTD) simulation of the system with RPB incidence, which is essential for plasmonic trapping. Trapping potential associated with force distribution was also calculated for the technical analysis. Extensive numerical simulations have subsequently been performed to study the effect of the gap distance of the proposed dimer structure on the electric filed enhancement. Lastly, we proposed a simple physical model based on simplified dipole approximation to understand the coupling mechanisms for the observed electric field enhancement in the proposed particle-particle-film system.

2. Theory and method

2.1 Virtual probe excited by focused RPB

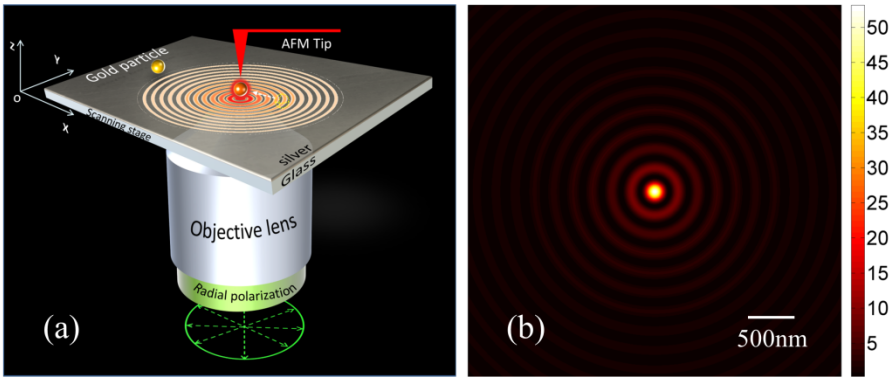

Fig. 1. (a) The proposed plasmonic trapping system. The incident light is linearly-polarized and is focused to a 45nm-thick silver film through a 1.49- NA objective lens. (b) Top-view of the plasmonic field (showing the z direction electrical-field distribution 10nm above the silver layer. z_0=1μm and $f_0 = 1$. The laser wavelength is 532 nm.

As described detail in [21] employing angular spectrum representation [27] and theory established by Richards and Wolf [28], the focal field can be obtained as follows,

$$E_{t,z}(\rho,\varphi,z) = \frac{ife^{-ik_1 f}}{2\pi}\int_0^{\theta_{\max}}\int_0^{2\pi} -E_{inc}(\theta,\phi)\cos\phi e^{ik_2\rho\sin\theta\cos(\phi-\varphi)}e^{i(k_{z1}-k_{z2})z_0}t^p e^{izk_{z2}}\frac{k_2^{\,2}}{k_1}\sin^2\theta\sqrt{\cos\theta}d\theta d\varphi \tag{1}$$

where ρ is the distance from the excitation point, φ is the angle with respect to the polarization direction and z is the distance to the metal film, f is the radius of Gaussian reference sphere for the incident beam, E_{inc} is the incident electrical field, k_1 and k_2 are the propagating wave vectors in the substrate and in the sample respectively, subscript z indicates the longitudinal component, Z_0 represents the distance from the laser focus to the metal film, and t^p is the transmission coefficient. According to the work by Q. W. Zhan [25,26], the longitudinal component is much stronger and dominates the total field distribution, which will be sued in our study here.

Our proposed plasmonic trapping system is shown in Fig. 1(a). The plasmonic field is excited on the Ag film by a focused radially polarized beam. As the surface plasmon is sensitive to TM polarization, a circle of light can excite surface plasmon on the Ag film, when they propagate to the center, a constructive interference will form a virtual probe with its maximum electrical filed at the center [Fig. 1(b)], which will be used to trap gold

nanoparticle. When the dimer structure is formed and fixed by both the trapped gold nanoparticle and the AFM tip, the scanning function can be achieved by the relative movement of the Ag film attached with solution sample.

Radially polarized doughnut mode can be synthesized with (1,0) mode.

$$\mathrm{RP} = \mathrm{HG}_{10}\,\mathbf{n}_x + \mathrm{HG}_{10}\,\mathbf{n}_y \tag{2}$$

To determine the focal fields of the other two doughnut modes we need to derive the focal fields for the y-polarized modes. This is accomplished by rotating the existing fields by 90° around the z-axis.

Expressing the coordinates $(x_\infty, y_\infty, z_\infty)$ by the spherical coordinates (f, θ, ϕ) we find the incident field of (1,0) mode

$$E_{inc} = E_0(2x_\infty / \omega_0)e^{-(x_\infty^2+y_\infty^2)/\omega_\infty^2} = (2E_0 f / \omega_0)\sin\theta\cos\phi e^{-f^2\sin^2\theta/\omega_0^2} \tag{3}$$

where $f_0 = \dfrac{\omega_0}{f\sin\theta_{\max}}$ is the filling factor. ω_0 represents the beam waist for the Gaussian beam and $f\sin\theta_{\max}$ is the aperture radius of the reference lens.

For simplification, we can write the exponential function as

$$f_\omega(\theta) = e^{-\frac{\sin^2\theta}{f_0^2\sin^2\theta_{\max}}} \tag{4}$$

This function is called the apodization function and can be viewed as a pupil filter.

Substitute the x- and y- polarized (1,0) mode incident field to the Eq. (1), we can get the focal field respectively as below,

$$E_{t,z}(\rho,\varphi,z) = \frac{ife^{-ik_1 f}}{2\pi}\int_0^{\theta_{\max}}\int_0^{2\pi} -(2E_0 f/\omega_0)f_\omega(\theta)\cos^2\phi e^{ik_2\rho\sin\theta\cos(\phi-\varphi)}e^{i(k_{z1}-k_{z2})z_0}t^p e^{izk_{z2}}\frac{k_2^2}{k_1}\sin^3\theta\sqrt{\cos\theta}d\theta d\phi \tag{5}$$

$$E_{t,z}(\rho,\varphi,z) = \frac{ife^{-ik_1 f}}{2\pi}\int_0^{\theta_{\max}}\int_0^{2\pi} -(2E_0 f/\omega_0)f_\omega(\theta)\sin^2\phi e^{ik_2\rho\sin\theta\cos(\phi-\varphi)}e^{i(k_{z1}-k_{z2})z_0}t^p e^{izk_{z2}}\frac{k_2^2}{k_1}\sin^3\theta\sqrt{\cos\theta}d\theta d\phi \tag{6}$$

The total focal field excited by focused radially polarized beam can be obtained by linear superposition of these two fields

$$E_{t,z}(\rho,\varphi,z) = \frac{ife^{-ik_1 f}}{2\pi}\int_0^{\theta_{\max}}\int_0^{2\pi} -(2E_0 f/\omega_0)f_\omega(\theta)e^{ik_2\rho\sin\theta\cos(\phi-\varphi)}e^{i(k_{z1}-k_{z2})z_0}t^p e^{izk_{z2}}\frac{k_2^2}{k_1}\sin^3\theta\sqrt{\cos\theta}d\theta d\phi \tag{7}$$

Using the mathematical identity $\int_0^{2\pi} e^{ix\cos(\phi-\varphi)} = 2\pi J_0(x)$, we can simplify this equation,

$$E_{t,z}(\rho,\varphi,z) = ife^{-ik_1 f}\int_0^{2\pi} -(2E_0 f/\omega_0)f_\omega(\theta)J_0(k_2\rho\sin\theta)t^p e^{i(k_{z1}-k_{z2})z_0}e^{izk_{z2}}\frac{k_2^2}{k_1}\sin^3\theta\sqrt{\cos\theta}d\theta \tag{8}$$

2.2 Modeling of RPB in FDTD simulation

For characterization of the optical interaction between nanoparticle and metallic film, Green's tensor approach [29,30], plasmon hybridization method [31,32], multiple-scattering method [33], FDTD [32,34], FEM [35] etc. have been introduced to make theoretical analysis. In this paper, we used FDTD method to simulate system with focused incident vector beam (i.e. RPB). Indirectly, RPB can be calculated as a user defined light source in the commercial FDTD software (Rsoft 8.1) with the following derivation. Mathematically, a left-handed and right-handed circularly polarized beam can be expressed as:

$$\vec{E}_{LHC} = A(r)\frac{\vec{e}_x + i\vec{e}_y}{\sqrt{2}} = \frac{A(r)}{\sqrt{2}} e^{i\phi}\left(\vec{e}_r + i\vec{e}_\phi\right) \tag{9}$$

$$\vec{E}_{RHC} = A(r)\frac{\vec{e}_x - i\vec{e}_y}{\sqrt{2}} = \frac{A(r)}{\sqrt{2}} e^{-i\phi}\left(\vec{e}_r - i\vec{e}_\phi\right) \tag{10}$$

RPB can be achieved by the superposition of a left-handed circularly polarized beam and a right-handed circularly polarized beam with a 2φ phase difference, where φ is the azimuthal angle,

$$\vec{E}_{Radial} = \vec{E}_{LHC} e^{-i\phi} + \vec{E}_{RHC} e^{i\phi} = \sqrt{2} A(r)\vec{e}_r \tag{11}$$

2.3 Force of metal particle by MST method and trapping potential calculation

The MST method has been described in detailed elsewhere including our previous work [21,24,36,37]. In a static electromagnetic field inside metal particle, the electrical field equals zero inside the metal particle, and only the surface of the particle has the electrical charge distribution. Thus we only need to consider the integration on the gold sphere surface, and the total average force can be calculated by the following expression

$$\left\langle \vec{F} \right\rangle = \left\langle \oint_s \vec{\vec{T}} \cdot \vec{n} ds \right\rangle \tag{12}$$

Where $\vec{\vec{T}} = \varepsilon \vec{E}\vec{E} + \mu \vec{H}\vec{H} - \frac{\vec{\vec{I}}}{2}\left(\varepsilon \left|\vec{E}\right|^2 + \mu \left|\vec{H}\right|^2\right)$ represents the Maxwell stress tensor matrix, ds is the integral area and $\vec{n}$ is the unit normal perpendicular to it.

Based on the electric field distribution obtained using the FDTD method, the MST formula can be employed to calculate the electromagnetic forces exerted on the Ag film, since both the electric and magnetic field components can be determined directly from the simulation data.

Trapping potential is used to determine the stability of the trap, which can be calculated by the following formula [38]

$$U(r_0) = \int_\infty^{r_0} \mathbf{F}(r) \cdot d\mathbf{r} \tag{13}$$

It means the trapping potential can be obtained if we get the force distribution in the radial direction. Generally, in order to overcome the motion from the thermal effects, more than 10 KT trapping potential depth is need for stable trapping [39], where K is the Boltzmann constant and T is the temperature.

2.4 Dipole approximation for single sphere and sphere dimer

For studying the behaviors of nanoparticles on the metallic film, simplified dipole approximation was used for analytical analysis, and it was used only to qualitatively explain the electrical field enhancement, while quantitative results were obtained using the FDTD. Radiative corrections will not be discussed in this approximation, and interested readers can refer to [40]. For single particle system as shown in Fig. 2(a), its polariability is

$$\alpha(\omega) = 4\pi R^3 \frac{\acute{U}(\omega) - \acute{U}_m}{\acute{U}(\omega) + 2\acute{U}_m} \tag{14}$$

where R is the radius of the sphere, $\acute{U}(\omega)$ is the permittivity of the sphere and $\acute{U}_m$ is the dielectric constant of the ambient.
The dipole moment of the sphere is

$$\mathbf{p} = \alpha \acute{U}_0 \acute{U}_m \mathbf{E} \tag{15}$$

where $\acute{U}_0$ is the permittivity of vacuum
The induced electrical field by the sphere is

$$\mathbf{E} = \frac{3(\mathbf{pg}\mathbf{r})\mathbf{r} - \mathbf{p}r^2}{4\pi \acute{U}_0 \acute{U}_m r^5} \tag{16}$$

According to [41], the absorption cross section and scattering cross section are as follows,

$$C_{abs}(\omega) = k \operatorname{Im}\alpha(\omega) \tag{17}$$

$$C_{sca}(\omega) = \frac{k^4}{6\pi}\left|\alpha(\omega)\right|^2 \tag{18}$$

where $k = |\mathbf{k}|$ is the wavenumber.

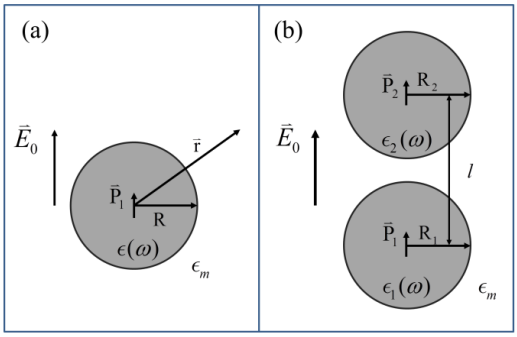

Fig. 2. Geometry of the dipole model: (a) single sphere; (b) vertical spheres dimer.

For a particle-particle system as shown in Fig. 2(b), their effective polarizability can be calculated by considering the induced electrical field influencing each other [42,43]. Since the incident electrical field is parallel to the axis of the dimer structure (i.e., the line connecting the centers of the dimer spheres), the local electric dipole field induced by the other particle is $p_2/(2\pi \acute{U}_0 \acute{U}_m l^3)$, so

$$\mathbf{E}_1^{loc} = \mathbf{E}_0 + \mathbf{p}_2/(2\pi \acute{U}_0 \acute{U}_m l^3) \tag{19}$$

$$\mathbf{E}_2^{loc} = \mathbf{E}_0 + \mathbf{p}_1/(2\pi \acute{U}_0 \acute{U}_m l^3) \tag{20}$$

Substituting the expressions for the dipole moments $\mathbf{p}_1 = \alpha \varepsilon_0 \varepsilon_m \mathbf{E}_1^{loc}$; $\mathbf{p}_2 = \alpha \varepsilon_0 \varepsilon_m \mathbf{E}_2^{loc}$ in equation above and solving the system of two coupled linear equations, we obtain the effective polarizability as follows,

$$\alpha_1^{eff} = \alpha_1 \frac{1 + \alpha_2 / (2\pi l^3)}{1 - \alpha_1 \alpha_2 / (2\pi l^3)^2} \tag{21}$$

$$\alpha_2^{eff} = \alpha_2 \frac{1 + \alpha_1 / (2\pi l^3)}{1 - \alpha_1 \alpha_2 / (2\pi l^3)^2} \tag{22}$$

The overall effective polarizability of the two particles

$$\alpha^{eff} = \frac{\alpha_1 + \alpha_2 + 2\alpha_1 \alpha_2 / (2\pi l^3)}{1 - \alpha_1 \alpha_2 / (2\pi l^3)^2} \tag{23}$$

3. Results

3.1 Optical force and trapping potential

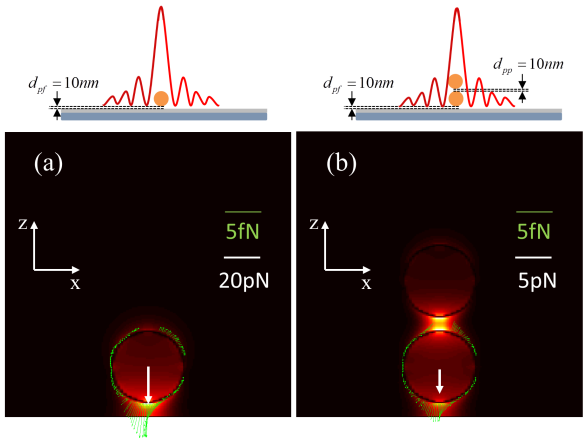

Fig. 3. The force analysis for: a single 50nm-diameter gold nanosphere: (a) placed on an Ag film; (b) a sphere is added to (a). The schematic diagrams show the locations of particles in the plasmonic field. d_{pp} and d_{pf} indicate the dimer gap distance and the particle-film gap dimer distance respectively. The green arrows show the forces at the points on the x-z section circle of the sphere. The white arrows indicate the total force as a result by the integral of the sphere surface. The background maps correspond to the electrical field.

Previously we have already demonstrated that 1 μm [24] and 200 nm gold nanoparticles [21] can be trapped by SP-VP. Here we will show that SP-VP can also be used for trapping 50-nm-diameter gold nanoparticle. Optical force is important for the bottom particle being maintained in close proximity to Ag film. First we calculated the force distribution via Eq. (12) with three dimensional electrical and magnetic fields data obtained from FDTD simulation, where the incident fields are unit peak normalized with power 1 W. As shown in Fig. 3, the force in x-z plane was used to represent the force distribution on the gold nanoparticle. Although both the incident light and the system have symmetry, the force distribution around the particle is still a bit asymmetrical, which may because of grid meshing. As shown in Fig. 3(a), the calculated total force is in z direction is -20.844 pN, and the forces in x and y direction are about one order of magnitude smaller.

We will now consider the situation when another gold nanoparticle intrudes from the top, e.g., a particle-particle dimer system, as shown in Fig. 3(b), the total force on the bottom particle of the dimer in z direction is -3.3561 pN, the forces in x and y direction are about two orders of magnitude smaller. The smaller total force comparing to the single particle [Fig. 3(a)] is weakened by the attracting force owning to the charges of the two polarized particles which is in positive z direction, which can be seen from the charge distribution in Fig. 7. However, the force at this level is still enough to control a nanoparticle above the silver film. About the force of the top particle, it is in negative z direction according the charge distribution in Fig. 8(b). In practical application, the top particle can be substituted by an AFM tip/probe, which is mechanically controllable.

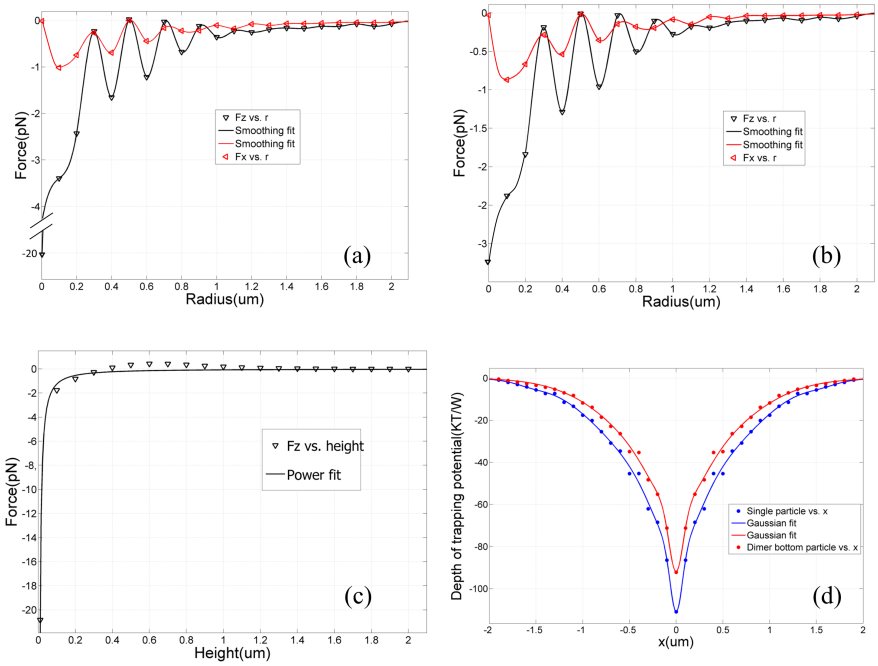

Fig. 4. The x- and z- direction total force distribution at the radial direction for (a) single particle above the Ag film and (b) vertically-oriented dimer above the Ag film, the bottom particle is studied. The parameters are same to Fig. 3. Radius is the particle offset length to the SP-VP center. The force was obtained every 100 nm. Both the particle-film and the particle-particle distances are 10 nm.The incident power is 1W. (c) The z- direction force distribution with different height (particle bottom to surface) the single particle at the center and off the Ag film. (d) The calculated trapping potential well along x direction for single particle (blue curve) and the bottom particle of the dimer (red curve).

Trapping potential is important for a stable trap of the bottom particle. According to Eq. (13), in order to obtain the trapping potential, we calculated the total forces distributions on the radial direction. As shown in Fig. 4, when the particle is away to more than 2 um, the forces become small closed to 0 because of the sharply attenuated the plasmonic field. The x- and z- direction forces in the Fig. 4(b) are both relatively weaken, but the distribution patterns remain unchanged. We made a conservative estimation of the trapping potential at the integral below 2um rather than infinity. Temperature is another factor in this estimation as heating effect important issue in the plasmonic trapping system [18]. However, in our configuration, the beam is out of focus by about 2-3μm thus the expected temperature change will not be significant. According to our previous temperature distribution calculation [24,36], the temperature increase in the focused plasmonic trapping system is estimated to be only about 2 Kelvin, as the gold metal film has a high thermal conductivity to dissipate the localized

heating. Note that the silver metal film used here has relatively higher thermal conductivity than gold [44]. Therefore we take the temperature as 300 K in the estimation. In the case of Fig. 4(a), the largest trapping potential is 111 KT/W at the center, which means that about 90 mw incident power can maintain a table trap. In the case of Fig. 4(b), the trapping potential well also exists at the center, which is 92.3 KT/W, which means more than 108.3 mw power can maintain a stable trap of a bottom particle. That is evidence that out proposed system works well.

In order to study the trapping stability, we calculated the trapping potential in the z-direction, as shown in Fig. 4(c). We can estimate the trapping potential value at the center is 115 KT/W, which is bigger than the radical direction trapping potential. Thus, the calculated minimum power can maintain 3 directions trap. We also calculated the trapping potential well as shown in the Fig. 4(d), there is no obvious local minima trapping well or barrier except the center, so center is the only possible trapping position for particle. But the position of an optically trapped particle is not fixed. Depending on the exact trap morphology and depth, the particle could be confined over a rather large region of space. According to the equipartition theorem the thermal kinetic energy of a particle can be related to the optical potential energy of a trap with stiffness k [45] $\frac{1}{2}KT = \frac{1}{2}k\left\langle x^2 \right\rangle$, where $\left\langle x^2 \right\rangle$ is the variance of the displacement from the equilibrium position. Assuming that the stiffness of the 50nm gold nanoparticle is 5.82 pN/nm/W [46], the square displacement $\left\langle x^2 \right\rangle$ at 300K can be estimated to be about 0.71 $\times 10^{-18}$ m^2, corresponding to a displacement of 0.8 nm, which is acceptable in the field enhancement. From the optical potential well we can make more rigorous estimation, the probability function for the displacement of a trapped particle can be deduced [47,48] $p(x) \propto \exp\left(\frac{-U(x)}{KT}\right) = \exp\left(\frac{-kx^2}{2KT}\right)$, The displacement x can be regarded as the position where the probability p(x) decrease to 1/e of the value p(0), which corresponds 0.43 KT trapping potential difference. Assuming the center has trapping potential 10KT, we can calculate the displacement is about 1.7 nm and 0.08 nm at x- and z- direction, respectively. Thus the impact of displacement on the field enhancement is acceptable.

3.2 Distance dependent field enhancements

Next, in order to study the SERS application of this vertical dimer system, we did the field enhancement calculation as well as two other structures as comparison. In single molecule SERS, the Raman enhancement factor is around 10^{12}, which suggests the electrical enhancement factor would have to be 10^3 according to equation $EF_{Raman} : \left|\frac{E_{loc}}{E_{in}}\right|^4$ [49], where E_{in} is the incident electric field, E_{loc} denotes the local electric field. Figure 5(a) shows the plasmonic field excited by the RPB. Without particle, the electric field enhancement factor is about 60 times. Comparing to traditional excitation method without SPP, we already obtain about one order of magnitude for the electrical enhancement. When a single particle is placed 10nm above the Ag film, the field enhancement is over 2×10^3. When a vertical dimer is placed 10 nm above the Ag film, since the RPB excited plasmonic field is almost longitudinal component which has the same orientation as the dimer, a much larger field enhancement of over 2×10^3 is observed at the dimer gap. It is interesting to see that the field enhancement at the dimer gap is larger than that at the particle-film gap at the same gap size. We noted that the electric field enhancement of the proposed vertical dimer is relatively smaller than that of a single trapped particle. This is expected because the total available energy has to be shared between particle-film gap and the particle-particle gap for the dimer configuration.

Nevertheless, both the vertical dimer and the trapped particle configurations lead to large field enhancement that is sufficient for high sensitive Raman applications such as single molecule detection. In addition, for the simple trapped particle configuration, the sample of interest has to be attached/close to the metal surface. The proposed vertical dimer configuration is a further extension of the trapped particle work with added flexibility. Figure 5(d) shows a horizontally-oriented dimer with particle size and same gap distance above the Ag film exited by the same plasmonic field, but the field enhancement is relatively lower , which is below 700 times. The hot spots locate at the bottom of the particles, because the incident field to this dimer is mainly longitudinal field of the SP-VP. This proves the vertically-dimer has better adaptability for field enhancement in some specific condition.

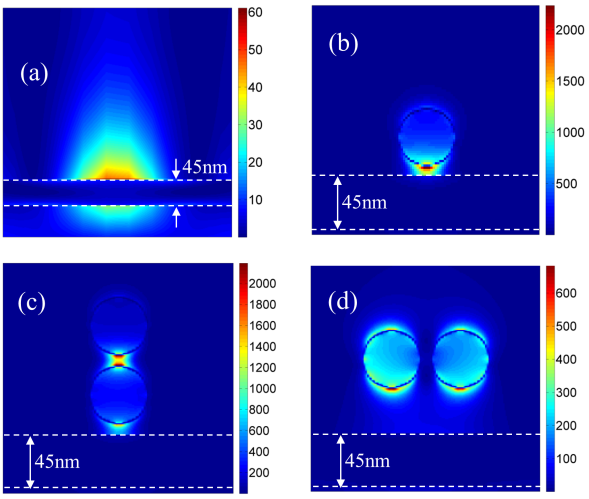

Fig. 5. The calculated electrical field enhancement in x-z plane, when: (a) no gold particles, (b) a vertical dimer placed on the Ag film and $d_{pf} = d_{pp} = 10nm$, (c) a horizontal dimer placed on the Ag film, the gap distance is same to 10nm and the height of the gap center is same to (b), which is 65nm from the surface.

In order to understand how the field enhancement depends on the particle-particle dimer gap distance d_{pp} and the particle-film gap distance d_{pf} , we performed more detailed calculations. As shown in Fig. 6(a), when d_{pf} is larger than 20 nm, the dimer gap enhancement becomes stable. Since 50 nm is in near-field within the SPP penetration depth, it can still excite the hot-spot in the dimer gap. When d_{pf} is lower than 20 nm, the situation becomes complex. Although the particle-film gap will absorb part of the energy and its field enhancement increases, the dimer gap enhancement is still higher than particle-film gap enhancement even when both d_{pp} and d_{pf} approaches 5 nm.

For further understanding of the situation when d_{pf} is below 20 nm, we made the measurement by varying d_{pp} from 1 nm to 20 nm with an interval of 1 nm. We studied 4 cases where d_{pf} was chosen to be 5 nm, 10 nm, 15 nm and 20 nm respectively. The results are showed in Fig. 6(b). As expected, the electrical field enhancement at the particle-film gap increases with the decrease of the d_{pf}. On the other hand, the electrical field enhancement at the particle-film gap increases with d_{pp}. This can be understood that the introducing of the top particle will influence the plasmonic coupling since some of the energy will be shared within the dimer. On the contrary, the average enhancement in the dimer gap decreases with d_{pf}. The

enhancement is inversely proportional to d_{pp} when d_{pp} is larger than 5 nm. However, when it becomes smaller than 5 nm, the results are irregular and become more complex. Since we used nonuniform grid after optimizing the calculation time, the grids in bulk area are 4 nm × 4 nm × 2 nm (2nm is in Z direction as the gaps are vertically-oriented that need to be more precise), the grids in edge area are 1 nm × 1 nm × 1 nm, this may be simulation errors come from grid meshing since the smallest grid size we used is 1 nm × 1 nm × 1 nm which is close to the 5-nm gap we studied here. It should be pointed out that the particle-film gap distance d_{pf} is within the plasmonic field penetration depth, which is typical around 10 nm. If we adjust d_{pp} to nanosize such as 5 nm, the enhancement is more than 7×10^3 times, which is enough for the single molecule SERS application.

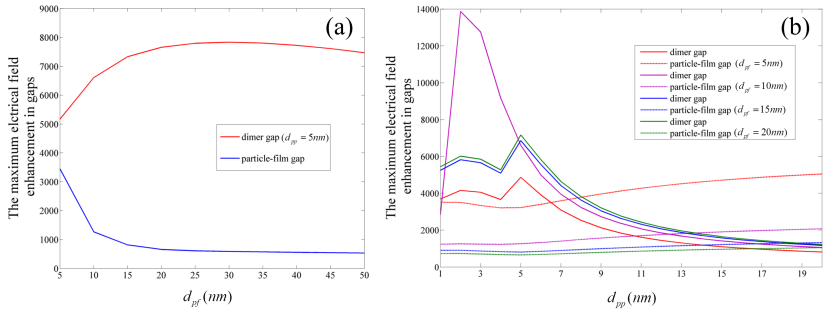

Fig. 6. The electrical field enhancement when changing d_{pf} (a) and d_{pp} (b) individually. The enhancement factor is obtained at the point next to the particle which will present the highest field value.

4. Discussion

In order to understand the underlying mechanism of the observed enhancement, we propose simple physical models based on the dipole approximation theory. As shown in Fig. 7(a), when the dimer is far away from the film, the dimer has little effect on the plasmonic field, thus it can be regarded as enhanced plasmonic field exciting the dimer. Although there is some decay along the z-direction [Fig. 5(a)], the enhancement is still relatively high in the dimer gap, indicating that the LSP-LSP coupling of the particle-particle interaction is strong. This mode corresponds to the result in Fig. 6(a) when d_{pf} is more than 20 nm.

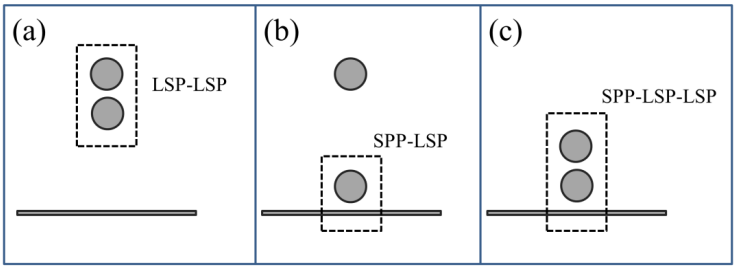

Fig. 7. Three plasmon hybridization modes: (a) dimer is far away from the film (d_{pf} >>R> d_{pp}); (b) the dimer gap distance is large and the one sphere is close to the film (d_{pp} >>R> d_{pf}); (c) dimer is close to the film ($d_{pp} \sim d_{pf}$ <R).

Figure 7(b) is the situation of mainly SPP-LSP coupling. The dimer gap distance is large and the bottom particle is close to the film. It can be considered that the two particles are

excited by the plasmonic field separately. Because of the absorption and scattering by the bottom particle, the field exerted on the top particle is weak. Thus the enhancement in the particle-film gap is stronger than that in the dimer gap when d_{pp} becomes large. This agrees with the result in Fig. 6(b). When the dimer gap and dimer-film gap size both become close to the particle size in the range of tens nanometers, SPP-LSP-LSP coupling appears [Fig. 7(c)]. The field enhancement within the dimer gap comes from the absorption and scattering of the plasmonic field. The absorption is proportional to dimer effective polarizibility according to Eq. (17), whilst the scattering is proportional to the square of the effective polarizability of the bottom particle. The field enhancement in the gap between the bottom particle and the film is from the absorption and scattering by the nanoparticle with the addition of the plasmonic field. The effective polarizability of the bottom particle is only part of total dimer effective polarizability, and the original plasmonic field is relatively small compared with these plasmon hybridizations. To sum up, that is reason why the dimer gap enhancement is large in this SPP-LSP-LSP thus our proposed vertical dimer system is of advantageous over a conventional particle-film system.

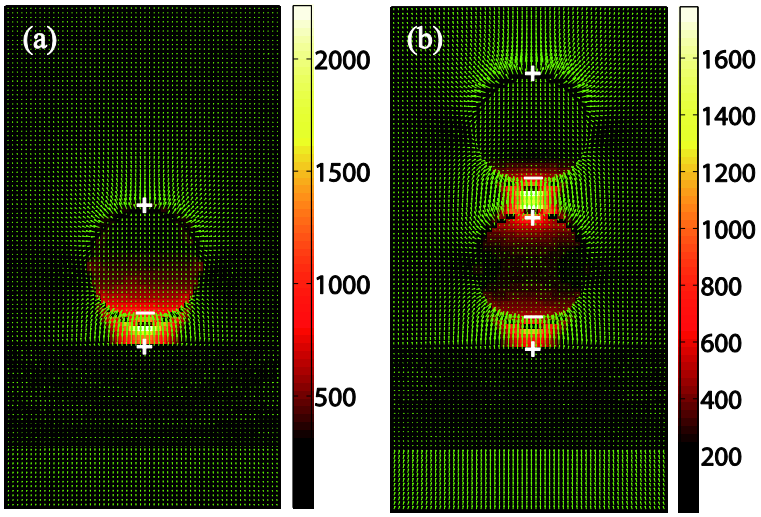

Fig. 8. The FDTD simulation for the electrical field line distribution of (a) a gold sphere placed above a silver film ($d_{pf} = 10nm$) and (b) gold nanosphere dimer ($d_{pp} = 10nm$) placed above a gold film ($d_{pf} = 10nm$). The color scale is the electrical intensity and it is same color bar for both.

Single nanoparticle or nanoparticle dimer far away from the Ag film can be analytically analyzed with dipole approximation introduced in the theory part, as they can be regarded as single nanosphere or two nanospheres in the uniform electrical excitation field. When these particles are close to the film surface, the SPP will engage and the plasmonic field varies intensely. Figure 8(a) and (b) shows the electrical field line distribution for a particle-film system and a particle-particle-film dimer system, respectively, using the SPP-LSP and SPP-LSP-LSP modes. In the diagram each electrical field line occupies 2 nm × 2 nm gridding, so the length of the electrical field line represents the charge density. In Fig. 8(a), the sign of the charge at the particle remains similar to a single polarized sphere [Fig. 2(a)]. However, since the plasmonic field decays from the surface, the charge density in the gap is larger than that at the top, as a result, the hot-spot locates at the gap rather than at the top.

As shown in Fig. 8(b), the electrical field lines change their direction and become more concentrated at the particle-particle dimer gap due to the introduction of the new particle at the top. Thus the free electrons at the bottom of the top particle and the top of the bottom

particle will have more intense interaction than that between the bottom particle and film. That's evidence that the localized plasmon hybridization dominates in this SPP-LSP-LSP mode. We can conclude that the vertically-oriented dimer structure within the particle-particle-film system is an effective and efficient SERS structure for imaging.

5. Conclusion

In conclusion, we presented, for the first time, a vertically-oriented dimer structure suitable for high sensitivity and scanning SERS application. We first demonstrated that a 50 nm gold nanoparticle could be trapped by SP-VP. Further force analysis indicates that the top particle will not influence the stable trapping of the bottom particle, which verified that the proposed system is feasible. Comparing to a horizontally-oriented dimer fabricated with complex technique, the vertically-oriented dimer is able to do scanning for Raman imaging and the dimer gap is under control. Moreover, we did the simulations with constructing incident RPB. Acting as the excitation field for the dimer, SP-VP is not only dominating in the longitudinal direction but also providing an enhanced field. The vertically-oriented dimer can effectively make use of the dominant longitudinal component of the SP-VP thus it can provide much stronger electric filed in the gap which is essential for high-sensitivity SERS applications. The electrical enhancement results show it is enough for single molecule detection SERS. In addition, we used the dipole approximation theory and simulated the gap distance dependent field enhancement at the same time. We found three main plamon coupling mechanisms. Through the electrical field line distribution, we obtained the charge distribution, which relates the Coulomb force and also reveal how the particles response in the plasmonic field. These coupling mechanisms will pave the way for exploiting SERS imaging application with more complex structure based on the proposed vertically-oriented dimer. Of course, there is some limitation in our current work, as we used fixed wavelength to do the calculation, which is not an optimized working wavelength. Since different wavelength source may bring different spectral responses, especially the resonance effects relate the nanostructure will make sense in the trapping force and the field enhancement. Our future work will do optimizing the working wavelength to satisfy both trapping potential and field enhancement, so that it can be better used in the practical application.